JOURNAL OF PROPULSION AND POWER
Vol. 20, No. 2, March–April 2004

Pulsed Plasma Thruster Plume Investigation Using a Current-Mode Quadruple Probe Method

Nikolaos A. Gatsonis,* Jurg Zwahlen,† and Adrian Wheelock‡
Worcester Polytechnic Institute, Worcester, Massachusetts 01609
and
Eric J. Pencil§ and Hani Kamhawi¶
NASA John H. Glenn Research Center, Cleveland, Ohio 44135

A current-mode quadruple-Langmuir-probe method was developed and used to measure electron temperature, electron density, and the ratio of ion speed to most probable thermal speed in the plume of a rectangular-plate laboratory model Teflon® pulsed plasma thruster. The current mode involves biasing all the electrodes and measuring the collected currents. The current collection theory and uncertainty analysis are presented. The thruster was operating at discharge energies of 5, 20, and 40 J and 15-microsecond pulses. Quadruple-probe measurements were taken at 10, 15, and 20 cm downstream of the Teflon propellant surface and angular locations of up to 40 deg off the centerline on planes perpendicular and parallel to the thruster electrodes. The electron temperature at 10 cm reaches values that range from 10 to 18 eV during the rise of the discharge current but remains below 5 eV for the rest of the pulse. The electron temperature shows no angular variation but reduces with increasing radial distance. The maximum electron density at 10 cm is $10,^{20}$ $7 \times 10,^{20}$ and 1.5×10^{21} m^{-3} for the 5, 20, and 40-J discharge energy, respectively. The electron density reduces with increasing angle especially at larger downstream distances. The ion-speed ratios indicate supersonic ions and increase with downstream distance and for all angles considered. Ion speeds at 10 cm are approximately 30,000 m/s at the beginning of the pulse and reduce in magnitude to below 10,000 m/s near the end of the pulse.

Nomenclature

A_p	=	probe area, m^{-2}
$A_{\parallel(\perp)}$	=	area for the parallel (perpendicular) to the flow electrode, m^{-2}
C_i	=	most probable ion velocity
d_s	=	probe sheath thickness, m
E_D	=	capacitor discharge energy, J
$I_{i(e)p}(t)$	=	ion, (electron) probe current, A
$I_p(t)$	=	total probe current, A
I_{sp}	=	specific impulse, s
$J_{i(e)0}$	=	ion, (electron) random current density, A/m^2
Kn_{st}	=	Knudsen number for species s-t collisions
k	=	Boltzmann's constant, 1.381×10^{-23} J/K
l_p	=	probe length, m
$m_{i(e)}$	=	mass of ion (electron), kg
$n_e(t)$	=	electron number density, m^{-3}
$n_e^{\max}(r, \theta)$	=	maximum electron density during a pulse, m^{-3}
r	=	radial distance downstream from the center of Teflon® surface, cm
r_p	=	probe radius, m
$S_i(t)$	=	ratio of ion speed to most probable ion velocity
s	=	probe spacing, m
$T_e(t)$	=	electron temperature, K
$T_e^{\max}(r, \theta)$	=	maximum electron temperature, eV
T_i	=	ion temperature
t	=	time, μs
$U_i(t)$	=	ion speed, m/s
Z_i	=	number charge of ion i
θ	=	polar angle measured from the center of the Teflon surface, deg
λ_D	=	Debye length, m
λ_{st}	=	mean free path for collisions between species s and t, m
τ_L	=	end-effect parameter
ϕ_p	=	potential of probe p, V
ϕ_s	=	plasma (or space potential), V
ϕ_{ps}	=	voltage difference between probe p and plasma potential, V
x_p	=	nondimensional potential at a probe p

Presented as Paper 2002-4123 at the AIAA/ASME/SAE/ASEE 38th Joint Propulsion Conference, Indianapolis, IN, 7 July 2002; received 7 April 2003; revision received 29 July 2003; accepted for publication 11 August 2003.

*Associate Professor, Mechanical Engineering Department, 100 Institute Road; gatsonis@wpi.edu. Senior Member AIAA.
†Graduate Research Assistant. Student Member AIAA.
‡Graduate Fellow. Student Member AIAA.
§Electrical Engineer, On-Board Power and Propulsion Branch. Associate Fellow AIAA.
¶Aerospace Engineer, Energy System Technology Branch. Member AIAA.

Introduction

THE characterization of pulsed-plasma-thruster (PPT) plumes is important for the investigation of plume/spacecraft interactions as well as for the understanding of the physical processes inside the thruster. A rectangular-geometry ablative PPT is an electromagnetic propulsion device shown schematically in Fig. 1. The main capacitor discharge ablates and ionizes the solid Teflon propellant. The generated plasma accelerates through electromagnetic and gasdynamic processes that are still not fully understood. The result of the Teflon decomposition and ionization processes in the PPT channel is an unsteady, partially ionized plume that consists of plasmoids emitted at the pulsing frequency of the thruster. Each plasmoid consists of neutrals and ions, material from electrode erosion, as well as electromagnetic fields and optical emissions. Various types of rectangular ablative PPTs have been flown successfully onboard spacecraft. The NOVA PPTs with peak power level of 30 W, I_{sp} of 543 s and I_{bit} of 400 mN-s and a combined operation of over 20 years, showed no observed impact on solar arrays or other spacecraft operations.[1] The Lincoln Experimental Satellite (LES) used four experimental PPTs for station keeping flawlessly

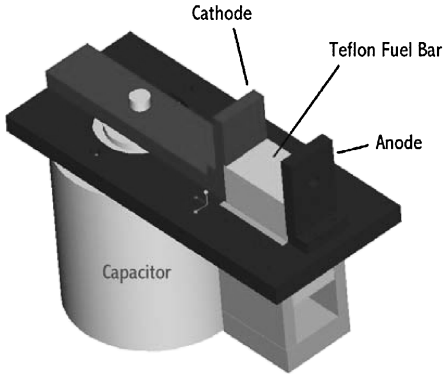

Fig. 1 Schematic of the laboratory PPT without the sputter guard (Gatsonis et al.).

for almost 9000 h (Ref. 2). The Earth Observer-1 (EO-1) satellite used PPTs without any observed adverse spacecraft interactions.[3] Numerous experimental investigations involved the LES-6 PPT,[4–6] and other specifically designed PPTs.[7–9] The renewed interest in the PPT prompted various investigations of the derivatives of the flight-qualified LES-8/9 PPT. These investigations provided an assessment of plume contamination,[10] plume materials and the neutral pressure evolution in the plume,[11] thrust measurements,[12] plume asymmetry,[13] particulate characterization,[14] as well as electron density and electron temperature.[15]

In this paper we present measurements of ion-speed ratio (ion speed and the most probable ion velocity), electron temperature, and electron density taken in the plume of a laboratory PPT using a quadruple Langmuir probe technique. The thruster used in this investigation is a rectangular model, derived from the heritage of flight-qualified LES-8/9 and EO-1 PPTs for which there has been no ion-speed characterization. Ion species production in the PPT channel is time dependent, and therefore, species populations in the plume are expected to have different mean velocities and temperatures. Such information is critical in the understanding of acceleration mechanisms in the PPT channel as well as in the assessment of possible plume/spacecraft interactions. Our knowledge is based on the early studies of Vondra et al. using the LES-6 PPT operating with discharge energies between 1 and 4 J (Ref. 4). They estimated an average exhaust speed of approximately 3000 m/s while Faraday cup measurements indicated an ion speed of approximately 40,000 m/s. The subsequent spectroscopic study of the LES-6 plume by Thomassen and Vondra[5] identified multiply ionized species with $C_{\mathrm{I}} \sim 5{,}000$–$15{,}000$ m/s, $C_{\mathrm{II}} \sim 20{,}000$–$30{,}000$ m/s, $C_{\mathrm{III}} \sim 30{,}000$–$40{,}000$ m/s, $F_{\mathrm{I}} \sim 5{,}000$–$15{,}000$ m/s, $F_{\mathrm{II}} \sim 15{,}000$–$25{,}000$ m/s, and $F_{\mathrm{III}} \sim 25{,}000$–$35{,}000$ m/s. These plume observations raised early on the awareness that in the PPT there is a slow component, mostly neutral, that contributes little to the useful thrust. Dawbarn et al.[16] using a PPT with ablated mass of $M_a = 1.71$ μg/pulse and a period of $P = 50$ μs observed two ion plasmoids moving with 40,000 and 13,000 m/s respectively. Studies of the LES-8/9 PPT plume used time-of-flight analysis of single Langmuir probe data and identified two ion speeds with approximately 30,000 and 60,000 m/s, respectively.[11] Fast ionization gauges detected the presence of slow neutral particles up to 1 ms after the end of the discharge.[11]

The laboratory PPT was operated at discharge energy levels of 5, 20, and 40 J that are relevant to several potential PPT applications.[17] The quadruple Langmuir probe is a hybrid between a triple probe introduced by Chen and Sekiguchi[18] and a crossed probe as appeared in Kanal.[19] In this paper we present a novel implementation for the quadruple probe, referred to as current mode that was proven suitable for the unsteady plume plasma. The current mode of the quadruple-probe operation involves biasing three probes and measuring the resulting currents. We also incorporate a current collection theory that improves the previous crossed-probe[19–21] implementations in flowing plasmas and quadruple-probe implementations in the plumes of magnetoplasmadynamic thrusters,[22] arcjets,[23] and gasdynamic PPTs.[24] These previous implementations used a current-collection theory that assumes negligible sheath thickness

Table 1 Operational characteristics of the laboratory-model PPT

Discharge energy, J	Impulse bit, μN-s	Mass loss/pulse, μg/pulse	Specific impulse, s
5.3	36	——	——
20.5	256	26.6	982
44.0	684	51.3	1360

($d_s/r_p \to 1$), assumes that the ion saturation current is independent of the applied potential and that the perpendicular probe operates in the ion-saturation regime. The quadruple-probe implementation of Burton and Bufton[23] in arcjets included corrections caused by multiple species. In our study the ion current collection to the parallel to the flow electrodes is based on the Peterson and Talbot[25] fits to Laframboise's[26] theory that accounts for effects of the sheath expansion on current collection. The perpendicular to the probe current utilizes the theory by Kanal[19] and includes contribution from electron and ion fluxes.

The quadruple-Langmuir-probe measurements were conducted in a large vacuum facility and covered the entire plume from the thruster centerline out to the backflow regions in both directions. The quadruple probe was attached to a translation stage that allowed data collection in the plume on two planes: perpendicular and parallel to thruster electrodes passing through the thruster's centerline. Measurements were obtained for radial distances of 10, 15, and 20 cm with respect to the center of the Teflon propellant face. The PPT itself was mounted on a rotational stage that allowed for polar angles of 0–180 deg. In this paper the current-mode quadruple-probe theory is outlined and probe construction, grounding scheme, as well as the cleaning procedure, are discussed. The data-reduction methodology, error analysis and temperature, density and ion speed ratio measurements are presented.

Thruster and Facility

A laboratory-model PPT with a parallel plate electrode arrangement and rectangular geometry housing was used in this study. The PPT is similar to the one flown on the EO-1 spacecraft and was designed at NASA Glenn Research Center for component life tests and plume characterization. The operational characteristics are shown in Table 1. The thruster has 2.5-cm-square electrodes, as shown in a schematic of the thruster (Fig. 1). The thruster uses a 33-μF capacitor for its main discharge and is capable of operating through a discharge energy range of 5–60 J. Experiments were conducted in a 2.13-m-diam, 3.05-m-long vacuum facility with a volume of 6.22 m^3 and an estimated pumping speed of 12,500 liters per second. The system used two oil diffusion pumps to achieve base pressures between 5×10^{-7} and 2×10^{-6} torr.

A test stand was designed and built that would allow the thruster to fire along the centerline of the vacuum tank, horizontally, from one end towards the other. This arrangement is illustrated in Fig. 2. The probe assembly was mounted on a horizontal translation table that was computer controlled. This allowed the probes to be moved horizontally downstream from the thruster exit plane remotely through a range of locations from within the exit plane to 20 cm downstream from the Teflon fuel bar surface. For off-centerline measurements the thruster itself was rotated on a computer-controlled rotational stage through the appropriate angle, with the probe aligned geometrically with the center of the Teflon fuel bar surface.

Current-Mode Quadruple Langmuir Probe Theory

A quadruple Langmuir probe is a combination of a triple Langmuir probe with a crossed probe, an electrode that is placed perpendicular to the plasma. The theory of operation of a triple Langmuir probe was first outlined by Chen and Sekiguchi[18] and the cross probe by Kanal.[19] A symmetric quadruple Langmuir probe, similar to the ones used in our experiments, consists of four identical probes placed in the plasma shown schematically in Fig. 3. In the typical mode of operation, referred to as voltage mode, one of the probes, indicated as probe 2 in Fig. 3a, is allowed to float in the plasma, and a fixed voltage $\phi_{13} = \phi_1 - \phi_3$ is applied between

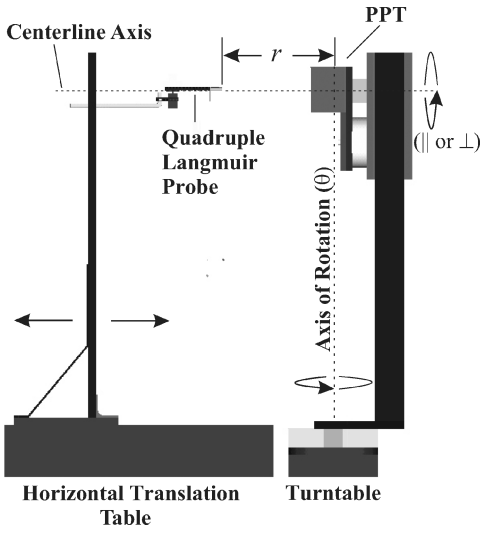

Fig. 2 Schematic of the laboratory PPT and the quadruple-Langmuir-probe motion system.

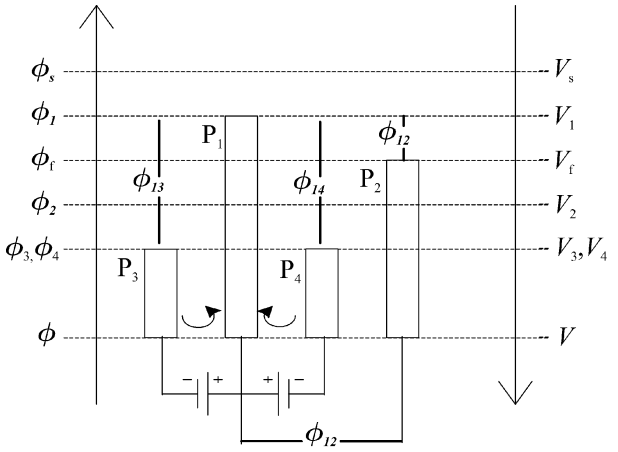

a) Voltage mode

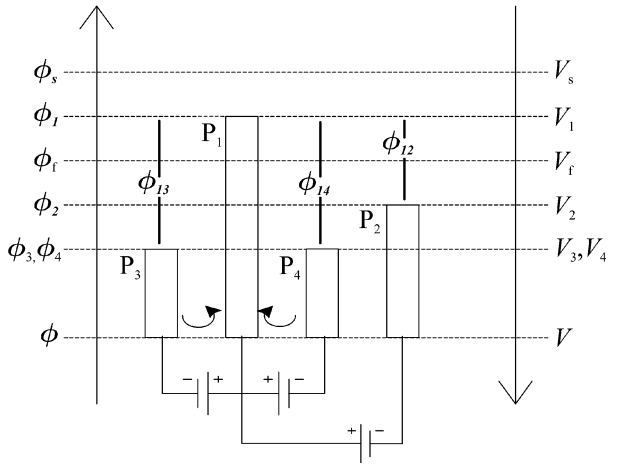

b) Current mode

Fig. 3 Electric diagram of a quadruple Langmuir probe.

the positive and negative probe with respect to the floating potential probe. The resulting voltage difference $\phi_{12}(t)$ and collected current $I(t)$ allow for the evaluation of $T_e(t)$ and $n_e(t)$. The perpendicular probe allows the determination of the ion-speed ratio between ion speed and the most probable ion velocity $S_i = u_i/C_i$.

Our previous experience of operation of triple probes showed that voltage measurement needed to obtain $\phi_{12}(t)$ is easily susceptible to electromagnetic interference (EMI) noise entering the system. We therefore extend here the current-mode triple Langmuir-probe operation to quadruple probes and referred to as the current-mode quadruple Langmuir probe illustrated in Fig. 3b. A fixed voltage ϕ_{12} is applied between probe 1 and probe 2, ϕ_{13} is applied between probe 1 and probe 3, and $\phi_{14} = \phi_{13}$ is applied between probe 1 and the perpendicular probe 4. The collected currents $I_1(t)$, $I_2(t)$, $I_3(t)$, and $I_4(t)$ allow for the evaluation of $T_e(t)$ and $n_e(t)$ and $S_i(t)$ as outlined next.

To develop the theory of the current-mode quadruple-probe operation, it is assumed that the probes are inserted in a two-temperature flowing plasma. The distribution function is a drifting Maxwellian:

$$f_q(\boldsymbol{r}, \boldsymbol{v}, t) = n_q(\boldsymbol{r}, t)\left(\frac{m_q}{2\pi k T_q}\right)^{\frac{3}{2}} \exp\left[-\frac{m_q(\boldsymbol{v}_q - \boldsymbol{U}_q)^2}{2kT_q}\right] \tag{1}$$

where m_q is the mass, v_t is the particle velocity, $n_q(\boldsymbol{r}, t)$ is the number density, $\boldsymbol{U}_q(\boldsymbol{r}, t) = \langle \boldsymbol{v}_q \rangle$ is the average (or drift) species velocity (brackets indicate average over the species distribution function), and T_t is the temperature for a species $q = e$ or $q = i$. We further assume that the angle between the flow velocity and the probe axis is given by an angle ϕ, and we define the speed ratio

$$S_q = (U_q/C_q) \tag{2}$$

where the most probable thermal speed is

$$C_t = \sqrt{2kT_t/m_t} \tag{3}$$

The quadruple-probe theory assumes that the probes are operating in the collisionless plasma,

$$r_p \ll \lambda_{ei}, \lambda_{ee}, \lambda_{en}, \lambda_{ii}, \lambda_{in} \tag{4}$$

and that the sheath is collisionless

$$d_s \ll \lambda_{ei}, \lambda_{ee}, \lambda_{en}, \lambda_{ii}, \lambda_{in} \tag{5}$$

It is also required that the sheath thickness is smaller than the interprobe spacing so that there are no sheath interactions between the probes

$$d_s < s \tag{6}$$

For a probe electrode at a potential less than the space potential ($\phi_p \leq \phi_s$) as shown in Fig. 3, the total probe current is

$$I_p = I_{ep} - I_{ip} \tag{7}$$

In writing the preceding equation, it is assumed that the electron current to a probe (retarded current) is positive and the ion current (accelerated current) to a probe negative. A probe therefore collects an electron current that is larger in magnitude than the ion current if $I_p > 0$.

The electron current to a probe aligned with the plasma flow ($\varphi = 0$ deg) is considered first. For a probe with $\phi_p \leq \phi_s$, the electrons are the repelled species, and the electron current is given by

$$I_{\|e} = A_p J_{e0} \exp\left[\frac{-e(\phi_s - \phi_p)}{kT_e}\right] = A_p J_{e0} \exp\left(\frac{-e\phi_{sp}}{kT_e}\right) \tag{8}$$

where the random electron current density to the probe is

$$J_{e0} = e n_e (kT_e/2\pi m_e)^{\frac{1}{2}} \tag{9}$$

The ion current to a cylindrical probe aligned with the flow operating in the collisionless regime depends on the Debye ratio r_p/λ_D, the ion speed ratio S_i, the temperature ratio $T_e/Z_i T_i$, and the nondimensional potential

$$\chi_p = \frac{e(\phi_p - \phi_s)}{kT_e} \tag{10}$$

The Debye length, assuming a quasi-neutral plasma $n_i \cong n_e$, is

$$\lambda_D = \sqrt{\varepsilon_0 kT_e / e^2 n_i} \tag{11}$$

For Debye ratios $5 \le r_p/\lambda_D \le 100$, $\chi_p > 3$, and $T_i/Z_i T_e \le 1$, Peterson and Talbot[25] give the ion current to a probe aligned with the flow ($\varphi = 0$ deg) by an algebraic fit to Laframboise's[26] data as

$$I_{\parallel i} = A_p J_{i0}(\beta + |\chi_p|)^{\alpha} \tag{12}$$

where

$$J_{i0} = en_i(kT_e/2\pi m_i)^{\frac{1}{2}} \tag{13}$$

The parameters α and β are given as

$$\alpha = 2.9/[\ell_n(r_p/\lambda_D) + 2.3] + 0.07(T_i/Z_i T)^{0.75} - 0.34 \tag{14}$$

$$\beta = 1.5 + (T_i/Z_i T_e)\left\{0.85 + 0.135[\ell_n(r_p/\lambda_D)]^3\right\} \tag{15}$$

The current collection by the perpendicular to the flow probe ($\varphi = 90$ deg) is based on the theory developed by Kanal.[19] The electron current is given by

$$I_{\perp e} = A_p J_{eo} \exp(-e\phi_{sp}/kT_e) \tag{16}$$

The ion current to the perpendicular probe for finite sheath thickness is given by Kanal[19] as a function of the speed ratio, the applied nondimensional potential, and the collection area. In the general case the collection area and nondimensional potential are not independent of each other. However, assuming negligible sheath thickness, that is, $d_s/r_p \gg 1$, Johnson and Murphree[20] developed an asymptotic expression

$$I_{\perp i} = A_{\perp} n_e e\left(\frac{kT_e}{2\pi m_e}\right)^{\frac{1}{2}} \frac{2}{\sqrt{\pi}} \exp\left(-S_i^2\right) \sum_{n=0}^{\infty} \left[\frac{S_i}{n!}\right]^2 \Gamma\left(n + \frac{3}{2}\right) \tag{17}$$

where the collector area becomes simply the probe area

$$A_{\perp} = 2\pi r_p L \tag{18}$$

Applying the current collection models with $A_1 = A_2 = A_3 \equiv A_{\parallel}$ and $A_4 = A_{\perp}$, we obtain the following system for the quadruple probe:

$$I_1 = A_{\parallel} J_{e0} \exp\left(-\frac{e\phi_{s1}}{KT_e}\right) - A_{\parallel} J_{i0}\left(\beta + \frac{e\phi_{s1}}{kT_e}\right)^{\alpha}$$

$$I_2 = A_{\parallel} J_{e0} \exp\left[-\frac{e(\phi_{s1} + \phi_{12})}{kT_e}\right] - A_{\parallel} J_{i0}\left[\beta + \frac{e(\phi_{s1} + \phi_{12})}{kT_e}\right]^{\alpha}$$

$$I_3 = A_{\parallel} J_{e0} \exp\left[-\frac{e(\phi_{s1} + \phi_{13})}{kT_e}\right] - A_{\parallel} J_{i0}\left[\beta + \frac{e(\phi_{s1} + \phi_{13})}{kT_e}\right]^{\alpha}$$

$$I_4 = A_{\perp} J_{e0} \exp\left[-\frac{e(\phi_{s1} + \phi_{14})}{kT_e}\right] - A_{\perp} n_e e\left(\frac{kT_e}{2\pi m_e}\right)^{\frac{1}{2}} \frac{2}{\sqrt{\pi}}$$

$$\times \exp\left(-S_i^2\right) \sum_{n=0}^{\infty} \left[\frac{S_i^n}{n!}\right]^2 \Gamma\left(n + \frac{3}{2}\right) \tag{19}$$

For $r_p/\lambda_D > 100$ Laframboise's theory is not formally applicable, and following Chen and Sekiguchi[18] the thin-sheath theory provides the ion current to a parallel probe by the well-known Bohm expression

$$I_{\parallel i} = A_{\parallel} en_e \sqrt{kT_e/m_i} \exp^{-\frac{1}{2}} \tag{20}$$

The system of equations (19) then becomes

$$I_1 = A_{\parallel} J_{e0} \exp\left(\frac{-e\phi_{s1}}{kT_e}\right) - A_{\parallel} en_e \sqrt{\frac{kT_e}{m_i}} \exp^{-\frac{1}{2}}$$

$$I_2 = A_{\parallel} J_{e0} \exp\left[\frac{-e(\phi_{s1} + \phi_{12})}{kT_e}\right] - A_{\parallel} en_e \sqrt{\frac{kT_e}{m_i}} \exp^{-\frac{1}{2}}$$

$$I_3 = A_{\parallel} J_{e0} \exp\left[\frac{-e(\phi_{s1} + \phi_{13})}{kT_e}\right] - A_{\parallel} en_e \sqrt{\frac{kT_e}{m_i}} \exp^{-\frac{1}{2}}$$

$$I_4 = A_{\perp} J_{e0} \exp\left[\frac{-e(\phi_{s1} + \phi_{14})}{kT_e}\right] - A_{\perp} n_e e\left(\frac{kT_e}{2\pi m_e}\right)^{\frac{1}{2}} \frac{2}{\sqrt{\pi}}$$

$$\times \exp\left(-S_i^2\right) \sum_{n=0}^{\infty} \left[\frac{S_i^n}{n!}\right]^2 \Gamma\left(n + \frac{3}{2}\right) \tag{21}$$

The solution to the system of nonlinear algebraic equations (19) or (21) provides S_i, n_e, T_e, and ϕ_{s1}. For $r_p/\lambda_D \gg 1$ Lam[27] has developed an asymptotic theory, but in our experiment the Debye ratios remained finite.

Diagnostics and Procedures

The quadruple probe is based on our previous triple probe design, modified to accommodate the crossed electrode shown schematically in Fig. 4 (Ref. 15). All electrodes are made of 0.127×10^{-3} m diam tungsten wire, passed through a 6.28×10^{-3} m diam alumina tubing sheath and expose 6×10^{-3} m to the plasma. Special shielding procedures were carried out to minimize any EMI effects on the cables running out of the tank. On the outside of the tank, the shielded cables are connected to BNC feedthroughs on a Faraday cage that houses the high-voltage power supply, triggering power supply, oscilloscope, probe biasing voltage sources, and the current probes. The cable shielding and Faraday cage were implemented from previous efforts to take voltage-based triple Langmuir-probe measurements in the PPT plume.[28]

A Rogowski coil was placed around the PPT's main discharge capacitor and used to measure the time derivative of the PPT discharge current. The integrated output from the Rogowski coil was recorded on the oscilloscope and used as a trigger for the data acquisition. The initiation of the PPT discharge as seen from the discharge current serve as a common zero time for all of the measurements. This can also be used in examining the global evolution of the PPT plume.

Within the Faraday cage the probe signal wires were connected to the quadruple-probe circuitry as shown in Fig. 5. The voltages ϕ_{13} and ϕ_{14} are each supplied by two 9-V batteries in series, and ϕ_{12} is supplied by two 1.5-V batteries in series. During a PPT pulse, ϕ_{12} was found to vary up to 50% while ϕ_{13} and ϕ_{14} by up to 20% their nominal value. The effects of these voltage variations in probe measurements are incorporated in the uncertainty estimation presented in the next section. The average voltages did not to change more than $\pm.01$ V for every 100 data sets collected. The voltages were also measured before and after each glow cleaning, with ϕ_{12} ranging from 2.876 to 2.989 V, and ϕ_{13} and ϕ_{14} ranging from 18.59 to 18.64 V. The currents to the quadruple-probe electrodes were measured with a current probe. The probe currents as well as the discharge current were recorded on a four-channel oscilloscope.

Over the course of numerous firings, the probe electrodes acquired a black residue from the Teflon plasma. The glow discharge method

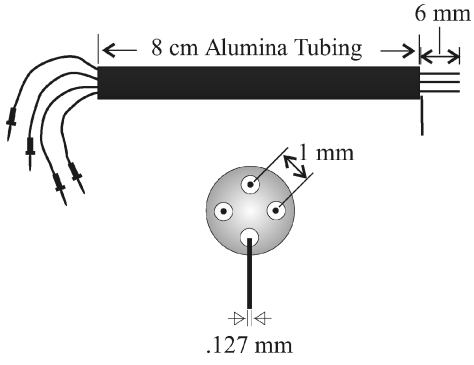

Fig. 4 Schematic of the quadruple Lamgmuir probe.

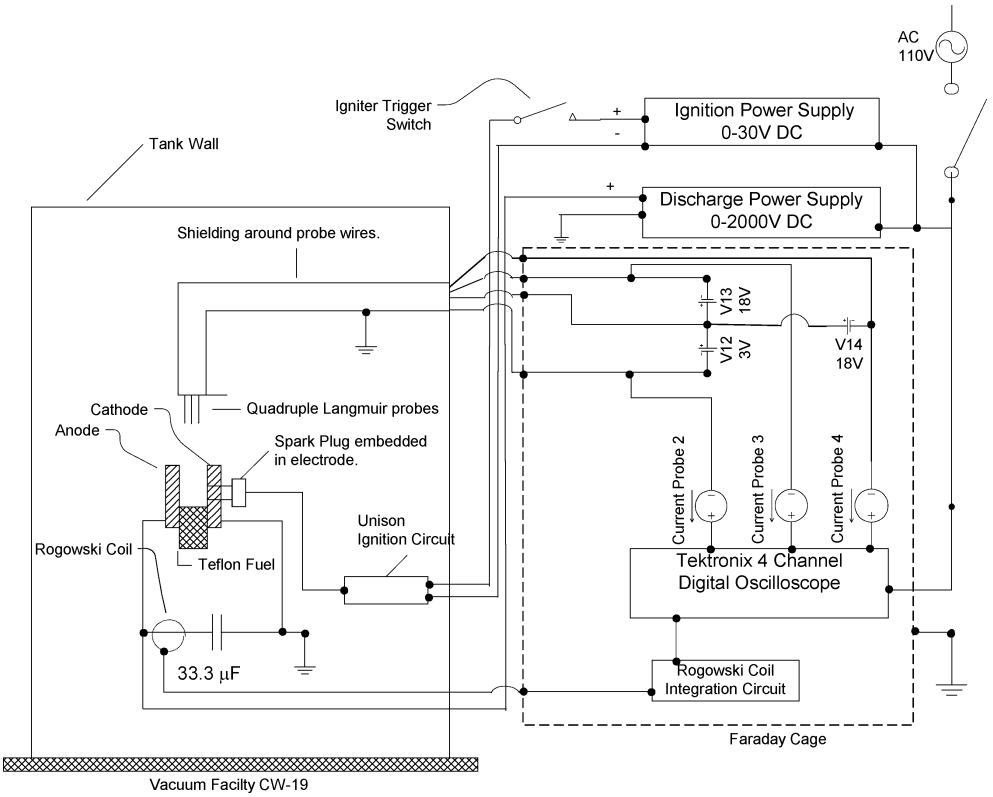

Fig. 5 Electronics diagram of the quadruple-Langmuir-probe experiment.

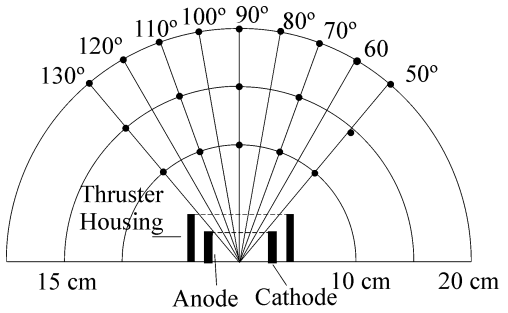

a) Plane perpendicular to the electrodes

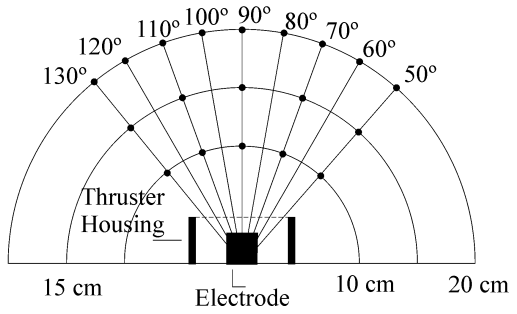

b) Plane parallel to the electrodes

Fig. 6 Measurement locations in the plume of the laboratory PPT.

described by Eckman et al.[15] was used to decontaminate the probes for every 30 pulses of thruster operation.

Quadruple-probe data were taken on the planes perpendicular and parallel to the thruster electrodes at locations shown in Fig. 6. For each discharge energy level of 5, 20, and 40 J, measurements were taken at 50, 70, 90, 110, and 130 deg at 10 and 15 cm from the Teflon fuel bar face and at 50, 60, 70, 80, 90, 100, 110, 120, and 130 deg at 20 cm from the Teflon fuel bar surface. At every spatial location and energy level the probe current was obtained by averaging signals from four consecutive PPT firings. Each current sample lasted for 20 ms and included 500 current measurements.

Sensitivity and Error Analysis

The implementation of the quadruple probe in the PPT plume requires careful consideration of plasma and probe parameters that enter in the evaluation of $T_e(t)$, $n_e(t)$, and $S_i(t)$. Estimates are obtained assuming that the PPT plume is composed of single-ionized C^+ and F^+ ions with mole fraction $[C^+]/[F^+] = 0.5$, electron temperature in the range of 1–10 eV, the electron density is in the range of 10^{18}–10^{21} m^{-3} and $0.01 \leq T_i/T_e \leq 1$.

Tables 2a and 2b shows that $6 \leq r_p/\lambda_D \leq 1700$ for the entire range of plasma parameters considered and the probes operate for the most part with $10 \leq r_p/\lambda_D \leq 100$, a range within the formal requirement of Laframboise's current-collection theory.[26] The sheath thickness needed to evaluate possible sheath interactions is estimated by[29]

$$d_s = \left(\sqrt{2}/3\right)\lambda_D (2e\phi_{ps}/kT_e)^{\frac{3}{4}} \tag{22}$$

The maximum probe potential with respect to the plasma is expected on probe 3 ϕ_{3s} and is estimated for the third probe to be between 25–60 V. Table 2 shows that no interference is expected between the sheaths because $45 \leq s/d_s \leq 14 \times 10^3$ for the range of plasma parameters considered.

The other requirement for the application of the current-collection theory is that the probe electrodes operate in the free-molecular regime, which implies $Kn_{st} = \lambda_{st}/r_p \gg 1$ for all type of collisions expected in the PPT plume. Charged-charged particle (e-i, i-i, e-e) and charged-neutral particle (i-n, e-n) collisions affect the ion and electron currents collected by a probe in flowing plasma. There has been no theory that consistently accounts for collisional effects on transitional probes, although many studies have identified several effects as reviewed in Chung et al.[30] It is evident from Table 2 that the quadruple-probe electrodes operate for the most part in the collisionless regime ($Kn_{st} = \lambda_{st}/r_p \geq 1$), although in certain cases the electrodes can be in the transitional regime. Ion–ion collisions in cases where $Kn_{ii} \leq 1$ account for an increase in ion current. Bruce and Talbot[31] measured an increase of approximately 10% in

Table 2a Nondimensional parameters of a quadruple Langmuir probe with $r_p = 1.25 \times 10^{-4}$ m and $s = 10^{-3}$ m in a PPT plum: Plasma parameter

	Plasma parameter			
Probe parameter	$n_e = 10,^{19}$ m^{-3} $T_e = 2$ eV, $T_i = 1$ eV	$n_e = 10^{19}$ m^{-3} $T_e = 5$ eV, $T_i = 1$ eV	$n_e = 10^{21}$ m^{-3} $T_e = 2$ eV, $T_i = 1$ eV	$n_e = 10^{21}$ m^{-3} $T_e = 5$ eV, $T_i = 1$ eV
r_p/λ_D	38.2	24.2	382.1	241.7
s/d_s	300.9	190.3	3008.9	1903.0
$Kn_{C+,C+}$	3.3	11.5	0.044	0.15
$Kn_{F+,F+}$	3.3	11.5	0.044	0.15
$Kn_{F+,C+}$	3.1	10.9	0.041	0.14
$Kn_{e,C+}$	74.7	408.3	1	5.2
$Kn_{e,F+}$	74.7	408.3	1	5.2
λ_{ei}/λ_D	2856.2	9868.0	376.5	1250.7
$Kn_{e,e}$	52.8	288.7	0.7	3.7
τ_L	203.9	203.9	2039.3	2039.3

Table 2b Nondimensional parameters of a quadruple Langmuir probe with $r_p = 1.25 \times 10^{-4}$ m and $s = 10^{-3}$ in a PPT plum: Neutral parameter

	Neutral parameter			
Probe parameter	$n_n = 10^{19}$ m^{-3} $T_n = T_i = 0.5$ eV	$n_n = 10^{19}$ m^{-3} $T_n = T_i = 1$ eV	$n_n = 10^{22}$ m^{-3} $T_n = T_i = 0.5$ eV	$n_n = 10^{22}$ m^{-3} $T_n = T_i = 1$ eV
$Kn_{C+,C}$	2792.1	3948.6	2.8	3.9
$Kn_{F+,F}$	4962.7	7016.9	5.0	7.0

the ion (saturation) current for an aligned probe with $Kn_{ii} \simeq 0.08$ and $\chi_p = -10$. Kirchhoff et al.[32] showed that for $\lambda_{ei} \geq 200\lambda_D$ or $Kn_{ei} \geq 200(\lambda_D/r_p)$ electron–ion collisions do not produce any transitional effects on the current with the probes in the retarding region, that is, with probe potentials between plasma and floating. Kirchhoff et al.[32] also showed that double probes can be used for the determination of electron temperature even when substantial collisional effects are present, probably because of cancellation effects. Bushman et al.[24] offer a similar explanation for quadruple probes. Charged-neutral collisions reduce the current collected by a probe below the collisionless limit predicted by Laframboise.[26] Kirchhoff et al.[32] discussed the effects of ion-neutral collisions on the ion current for a probe in the ion-saturation regime and the effects of electron-neutral collisions on the electron current for probes in the retarding-field regime. Clearly, Tables 2a and 2b shows that the effects of ion-neutral and electron-neutral collision can be ignored.

The triple probe was aligned with the polar angle measured from the center of the Teflon surface, which might have resulted in probe misalignment with the flow vector. These issues have been discussed by Eckman et al.,[15] where it was argued that the effects of misalignment would not adversely affect triple-probe measurements. The end-effects parameters given by

$$\tau_L = (L_p/\lambda_D)(kT_e/m_i)^{\frac{1}{2}} U_i^{-1} \tag{23}$$

are estimated in Tables 2a and 2b using a maximum ion speed of $U_i = 30,000$ m/s. The $\tau_L \gg 50$ ensures that end effects are negligible and that the ion current is not sensitive to any small misalignments between the probe and the flow vector.

The uncertainties in $T_e(t)$, $n_e(t)$, $\phi_{s1}(t)$, and $S_i(t)$, designated as $\Delta T_e(t)$, $\Delta n_e(t)$, $\Delta\phi_{s1}(t)$, and $\Delta S_i(t)$, depend on the propagation of uncertainties of all of the parameters entering in their evaluation through the system of equations (21). However, the system (21) is in implicit form, nonlinear, and therefore uncertainty analysis is beyond the methodology presented in literature.[33] The system (21) is written in the form

$$\begin{aligned}
f_1(T_e, n_e, \phi_{s1}, S_i, r_p, l_p, m_i) &= I_1 \\
f_2(T_e, n_e, \phi_{s1}, S_i, r_p, l_p, m_i, \phi_{12}) &= I_2 \\
f_3(T_e, n_e, \phi_{s1}, S_i, r_p, l_p, m_i, \phi_{13}) &= I_3 \\
f_4(T_e, n_e, \phi_{s1}, S_i, r_p, l_p, m_i, \phi_{14}) &= I_4
\end{aligned} \tag{24}$$

Upon differentiation the preceding system becomes

$$\begin{aligned}
&\frac{\partial f_1}{\partial T_e}\Delta T_e + \frac{\partial f_1}{\partial n_e}\Delta n_e + \frac{\partial f_1}{\partial \phi_{s1}}\Delta\phi_{s1} + \frac{\partial f_1}{\partial S_i}\Delta S_i \\
&\quad = -\left(\frac{\partial f_1}{\partial m_i}\Delta m_i + \frac{\partial f_1}{\partial l_p}\Delta l_p + \frac{\partial f_1}{\partial r_p}\Delta r_p\right) + \Delta I_1 \\
&\frac{\partial f_2}{\partial T_e}\Delta T_e + \frac{\partial f_2}{\partial n_e}\Delta n_e + \frac{\partial f_2}{\partial \phi_{s1}}\Delta\phi_{s1} + \frac{\partial f_2}{\partial S_i}\Delta S_i \\
&\quad = -\left(\frac{\partial f_2}{\partial m_i}\Delta m_i + \frac{\partial f_2}{\partial l_p}\Delta l_p + \frac{\partial f_2}{\partial r_p}\Delta r_p + \frac{\partial f_2}{\partial \phi_{12}}\Delta\phi_{12}\right) + \Delta I_2 \\
&\frac{\partial f_3}{\partial T_e}\Delta T_e + \frac{\partial f_3}{\partial n_e}\Delta n_e + \frac{\partial f_3}{\partial \phi_{s1}}\Delta\phi_{s1} + \frac{\partial f_3}{\partial S_i}\Delta S_i \\
&\quad = -\left(\frac{\partial f_3}{\partial m_i}\Delta m_i + \frac{\partial f_3}{\partial l_p}\Delta l_p + \frac{\partial f_3}{\partial r_p}\Delta r_p + \frac{\partial f_3}{\partial \phi_{13}}\Delta\phi_{13}\right) + \Delta I_3 \\
&\frac{\partial f_4}{\partial T_e}\Delta T_e + \frac{\partial f_4}{\partial n_e}\Delta n_e + \frac{\partial f_4}{\partial \phi_{s1}}\Delta\phi_{s1} + \frac{\partial f_4}{\partial S_i}\Delta S_i \\
&\quad = -\left(\frac{\partial f_4}{\partial m_i}\Delta m_i + \frac{\partial f_4}{\partial l_p}\Delta l_p + \frac{\partial f_4}{\partial r_p}\Delta r_p + \frac{\partial f_4}{\partial \phi_{13}}\Delta\phi_{13}\right) + \Delta I_4
\end{aligned} \tag{25}$$

The partial derivatives in the preceding system are the sensitivity coefficients and are obtained analytically. The system (25) is solved numerically for $\Delta T_e(t)$, $\Delta n_e(t)$, $\Delta\phi_{s1}(t)$, and $\Delta S_i(t)$. We proceed next with the evaluation of ΔI_1, ΔI_2, ΔI_3, ΔI_4, Δr_p, Δl_p, $\Delta\phi_{12}$, $\Delta\phi_{13}$, $\Delta\phi_{14}$, and Δm_i.

The uncertainties ΔI_1, ΔI_2, ΔI_3, and ΔI_4 are set equal to the sensitivity of the current probes used in the experiment. The sensitivity values are taken to be $\pm 2.0\%$ of the full-scale probe current measured on the oscilloscope, that is, $\Delta I_1 = \pm 0.02 I_{1\text{F.S.}}$, $\Delta I_2 = \pm 0.02 I_{2\text{F.S.}}$, and $\Delta I_3 = \pm 0.02 I_{3\text{F.S.}}$. The uncertainties in $\Delta\phi_{12}$, $\Delta\phi_{13}$, $\Delta\phi_{14}$ arise from the variation of the applied voltages during the PPT pulse. To determine this variation, the applied voltages were measured at $r = 20$ cm on the centerline at discharge energy levels of 5, 20, and 40 J, respectively.

Table 3 Mean, standard error, and 95% confidence interval for the applied potentials $\phi_{12}(t)$, $\phi_{13}(t)$, and $\phi_{14}(t)$ measured at r = 20 cm in the plume of a laboratory PPT

E_D, J	$\bar{\phi}_{12}$, V	$s(\bar{\phi}_{12})$, V	$\Delta\bar{\phi}_{12}$, V	$\bar{\phi}_{13}$, V	$s(\bar{\phi}_{13})$, V	$\Delta\bar{\phi}_{13}$, V	$\bar{\phi}_{14}$, V	$s(\bar{\phi}_{14})$, V	$\Delta\bar{\phi}_{14}$, V
5	3.396	0.086	±0.169	19.166	0.038	±0.075	18.672	0.039	±0.077
20	3.117	0.039	±0.076	18.982	0.046	±0.091	17.958	0.059	±0.115
40	3.390	0.089	±0.175	18.078	0.066	±0.130	17.269	0.100	±0.196

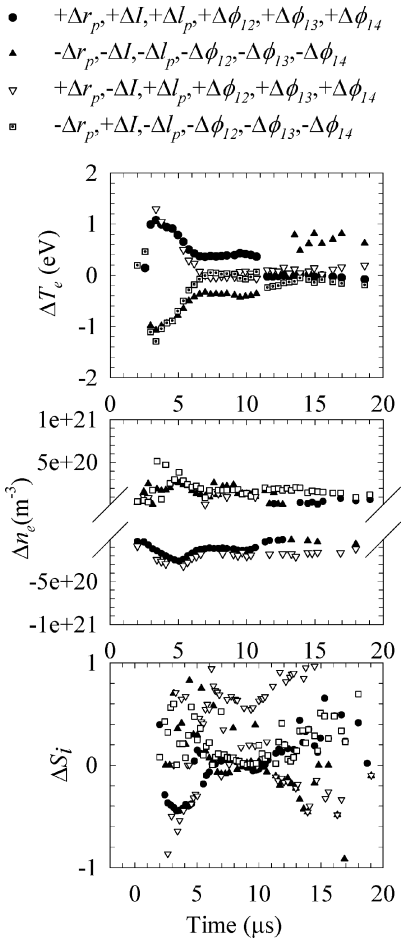

Fig. 7 Errors $\Delta T_e(t)$, $\Delta n_e(t)$, and $\Delta S_i(t)$ for combinations of uncertainties from quadruple Langmuir-probe-measurements taken at r = 10 cm on the centerline in the plume of a 40-J laboratory PPT.

Table 3 presents the mean, the standard deviation, and the 95% confidence interval about the mean given as

$$\Delta\bar{\phi}_{1p} = \pm t(v, z)s(\bar{\phi}_{1p}) \tag{26}$$

where $t(v, z)$ is the t statistic for $v = n - 1$ degrees of freedom and $z = 1.96$ (Ref. 34). This analysis provides the uncertainties that are evaluated as $\Delta\phi_{1p} = \Delta\bar{\phi}_{1p}$. In addition, in the solution of the system (24) the mean voltages $\bar{\phi}_{12}$, $\bar{\phi}_{13}$, and $\bar{\phi}_{14}$ are used in place of ϕ_{12}, ϕ_{13}, and ϕ_{14}, respectively. The uncertainties Δr_p and Δl_p are set equal to the precision of the calipers used in the construction of the probes as $\Delta r_p(t) = \Delta l_p(t) = \pm 0.0254 \times 10^{-3}$ m.

The next step in the evaluation of the errors $\Delta T_e(t)$, $\Delta n_e(t)$, and $\Delta S_i(t)$ involves the assessment of the right-hand sides in the system (25) that contain contributions from the uncertainties. An analysis was performed where the right-hand sides were evaluated for individual uncertainty terms assuming all remaining uncertainty terms were set to zero and then calculating the resulting absolute errors $|\Delta T_e(t)|$, $|\Delta n_e(t)|$, and $|\Delta S_i(t)|$ from Eqs. (25). This analysis revealed that the dominant contributors to $|\Delta T_e(t)|$ and to $|\Delta S_i(t)|$ are $\pm\Delta I_1$, $\pm\Delta I_2$, $\pm\Delta I_3$, and $\Delta\bar{\phi}_{12}$, whereas the dominant contributor to $|\Delta n_e(t)|$ is $\pm\Delta r_p$. The analysis also revealed that by changing the sign of an uncertainty term the sign of the error changes. Effects of combinations of uncertainty terms on $\Delta T_e(t)$, $\Delta n_e(t)$, and $\Delta S_i(t)$ were also evaluated following a similar process. It was concluded that the combination of $(-\Delta I, +\Delta r_p, +\Delta I_p, +\Delta\phi_{12}, +\Delta\phi_{13}$, and $+\Delta\phi_{14})$ resulted in the maximum errors $\Delta T_e(t)$, $\Delta n_e(t)$, and $\Delta S_i(t)$. Figure 7 shows the evaluation of maximum errors for a typical data set.

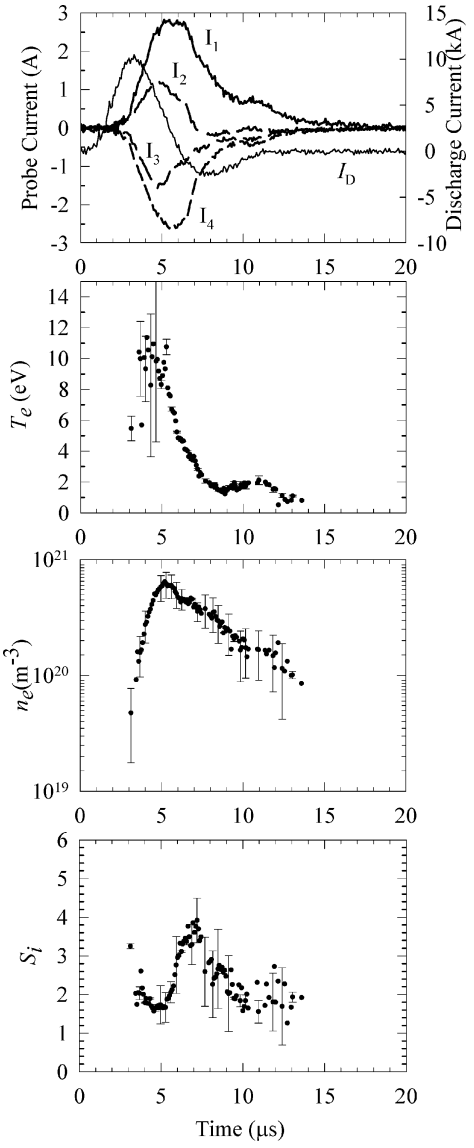

Fig. 8 Discharge current, quadruple-Langmuir-probe currents, and the resulted $n_e(t)$, $T_e(t)$, $S_i(t)$ with maximum error bars. Measurements taken at r = 10 cm along the centerline (θ = 90 deg) in the plume of a 20-J laboratory PPPT.

The plume plasma is assumed to be composed of a single ion species with an equivalent mass of $m_i = 16.66m_p$. This is consistent with the assumption of complete decomposition of Teflon and the presence in the plume of single-ionized C^+ and F^+ ions with a mole fraction of $[C^+]/[F^+] = 0.5$. Therefore, $\Delta m_i = 0$.

Data Analysis and Discussion

For each set of currents $I_1(t)$, $I_2(t)$, $I_3(t)$, measured at a specified position (r, θ) and discharge energy E_D, the procedure to determine $T_e(t)$, $S_i(t)$, $T_e(t)$ is the following:

1) Eliminate data points with currents below the sensitivity of the current probes.

2) Obtain an initial guess for T_e^0, n_e^0, and S_i^0 from the thin sheath equations, and use that to evaluate the ratio r_p/λ_D. Obtain $T_e(t)$, $S_i(t)$, $T_e(t)$ from the solution of Eqs. (19) for $r_p/\lambda_D \leq 100$ or from Eq. (21) for $r_p/\lambda_D > 100$.

3) Obtain the errors $\Delta T_e(t)$, $\Delta n_e(t)$, and $\Delta S_i(t)$ from the solution of Eqs. (25).

4) Remove outliers from $T_e(t)$ data through a regression analysis that identifies data points with standardized residuals with values larger than ± 2.

Typical quadruple-Langmuir-probe measurements taken at $r = 10$ cm on the centerline ($\theta = 90$ deg) of the 20-J laboratory PPT plume are shown in Fig. 8 along with the resulting electron temperature, electron density, and ion-speed ratio. The capacitor discharge lasts for approximately 12 μs, and the discharge current has a peak of 10.45 kA at $t = 3.3$ μs followed by a current reversal that has a secondary peak of -2.66 kA at $t = 8.26$ μs. The current reversal starts at $t \simeq 6.1$ μs so the pulse is split almost equally between the main and the secondary discharge. These are characteristics common to all discharge currents recorded at 20 and 40 J. Figure 8 shows that current collection by the probes at $r = 10$ cm begins at $t \simeq 2$ μs and continues for up to $t \simeq 15$ μs, approximately 3 μs after the end of the discharge. Figure 8 shows that probe 1 and probe 2 collect mostly electrons,whereas probe 3 and probe 4 collect mostly ions. The peaks in collected probe currents are $I_1^{\max}$ ($r = 10$, $\theta = 90$) $= 2.8188$ A at $t = 5.46$ μs; $I_2^{\max}$ ($r = 10, \theta = 90$) $= 1.2465$ A at $t = 4.74$ μs; $I_3^{\min}$ ($r = 10$, $\theta = 90$) $= -1.5614$ A at $t = 4.74$ μs; and $I_4^{\min}$ ($r = 10$; $\theta = 90$) $= -2.6115$ A at $t = 5.46$ μs.

The electron temperature in Fig. 8 increases from 5.46 ± 0.79 eV at $t = 3.12$ μs to reach a maximum of $T_e^{\max}$ ($r = 10$, $\theta = 90$) $= 11.5 \pm 3.1$ eV at $t = 4.08$ μs indicating the presence of hot electrons associated with the peak of the discharge. A secondary peak of 2.12 ± 0.28 eV is observed to occur at $t = 10.96$ μs and is associated with the reversal of the discharge current. The electron density has a maximum of $n_e^{\max}$ ($r = 10$, $\theta = 90$) $= 6.4 \times 10^{20} \pm 1.8^{20}$ m^{-3} at $t = 5.2$ μs, about 1 μs after the temperature peak. The ion speed ratio has a maximum of $S_i^{\max}$ ($r = 10, \theta = 90$) $= 3.91 \pm 0.58$ at $t = 7.2$ μs.

The 20-J measurements taken at $r = 10$ and 20 cm are shown in Fig. 9 for the parallel and in Fig. 10 for the perpendicular planes, respectively. On both planes the electron temperature measured at $r = 10$ cm has a maximum after the peak of the discharge current and reduces to below 4 eV for times greater than 6 μs. This indicates

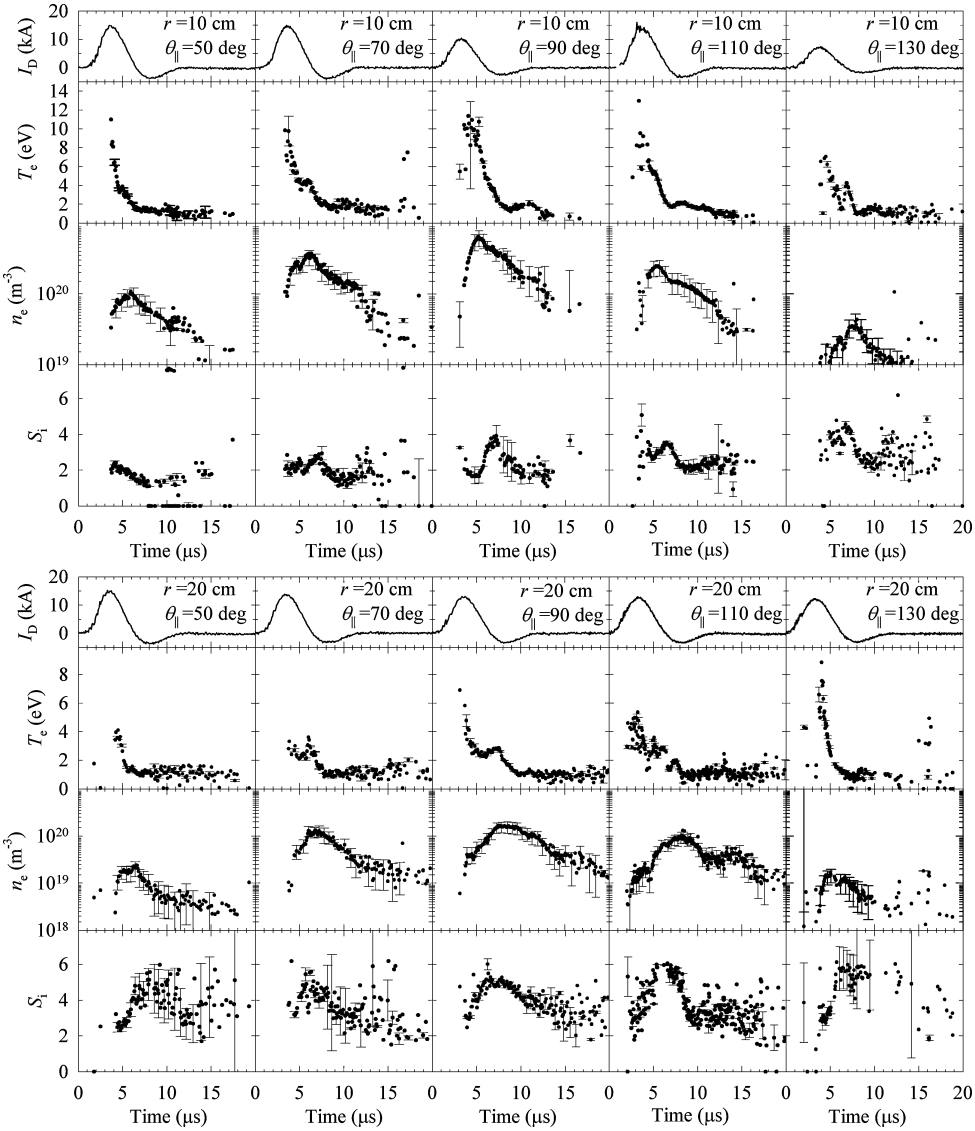

Fig. 9 Electron temperature, electron density, and ion-speed ratio from quadruple-Langmuir-probe measurements taken on the parallel to the electrodes plane, in the plume of a 20-J laboratory PPT.

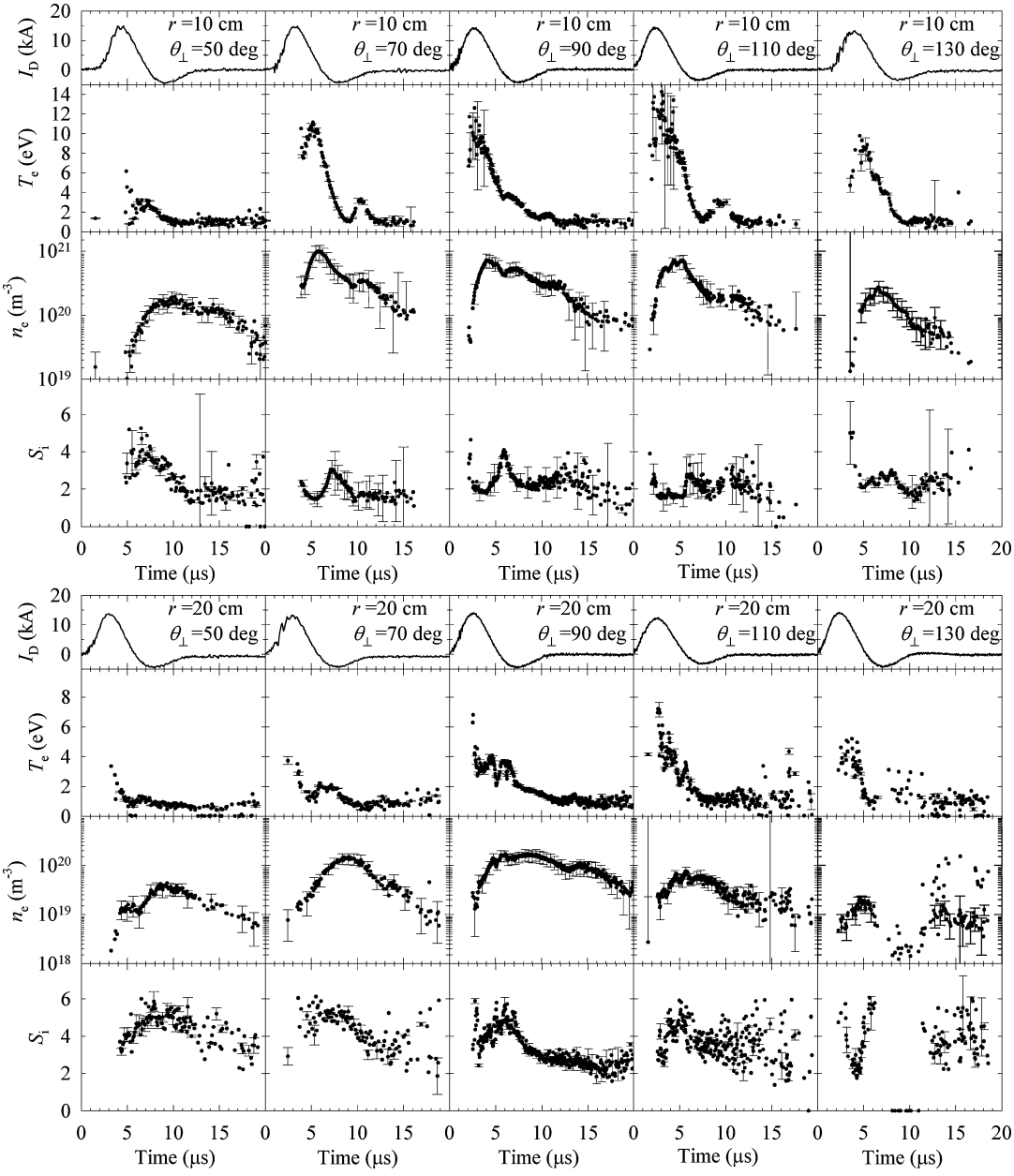

Fig. 10 Electron temperature, electron density, and ion-speed ratio from quadruple-Langmuir-probe measurements taken on the perpendicular to the electrodes plane, in the plume of a 20-J laboratory PPT.

that near-exit measurements taken during the main capacitor discharge show the presence of 12-eV electrons, whereas measurements taken after the main discharge are consistent with electrons with temperatures below 4 eV. Furthermore, in certain cases the discharge reversal can be related with a secondary peak in electron temperature. We could, therefore, associate these hot electrons with the capacitor discharge because it is well known that in arc discharges where electric fields are strong the electron temperature can be much higher than the temperature of the gas itself.[35] Similar observations by Eckman et al.[15] indicated high electron temperatures at the beginning of the pulse. However, Eckman et al. smoothed out the noisy measurements taken before the peak of the discharge current and as a result reported for the 20-J laboratory PPT maximum electron temperatures below 4 eV. In the present study the fidelity of the quadruple-Langmuir-probe technique allowed the analysis of measurements for the full duration of the discharge without need for smoothing of the currents. A regression analysis was used to remove a few temperature outliers with standardized residuals larger than ± 2. It is therefore possible for even higher temperatures to exist during the main discharge especially at distances closer to the thruster exit. The experiments of Vondra et al.[4] using single Langmuir probes reported electron temperatures ranging from 20–25 eV and attributed to the capacitor breakdown. To substantiate the quadruple-probe measurements, the ratios of the electric field to gas pressure (E/p) that would be present in the PPT were obtained from simulations of the PPT channel flow. These simulations were performed using a version of the MACH2 magnetohydrodynamic code implemented for the PPT with an ablation model.[36] The 20-J simulation provided an (E/p) range from 0.1–260 V/cm-mmHg during the discharge. Measurements in monatomic and diatomic gases with (E/p) in the range from 0–100 V/cm-mmHg clearly indicate the possible large differences between the electron and heavy species temperature.[37]

Figures 9 and 10 show that the electron temperature in both planes exhibits almost no angular variation for the radial distances considered. However, the electron temperatures decrease with increasing distance for each of the angles considered. This behavior is consistent with a cooling process of the expanding plasmoid.

The electron density in Figs. 9 and 10 is highest at the centerline and reduces with increasing angle especially at larger downstream distances. The density at $r = 20$ cm is almost an order of magnitude smaller than at $r = 10$ cm for all angles considered.

The ion-speed ratio plotted in Figs. 9 and 10 show that the ions at $r = 10$ cm are supersonic for all angles considered. The ion-speed ratio increases with downstream distance overall and for all angles. The increase can be attributed to both an increase in ion speed and reduction in temperature. The attributes shown in Figs. 9 and 10 for the 20-J discharge are similar to those from measurements taken at 5-J and 40-J discharge energies.[38]

The effects of discharge energy on plume parameters are examined in Fig. 11. Two data sets taken on the centerline are plotted for distances of 10 and 20 cm from the Teflon surface. The electron temperature and density increase with energy level, but the speed ratios remain almost insensitive to the discharge energy. The hot electrons associated with the main discharge are present at all energy levels. Maximum electron temperature at $r = 10$ cm is 10 ± 1.3 eV for the 5-J discharge, 10.8 ± 0.5 eV for the 20-J discharge, and 13.5 ± 1.8 eV for 40-J discharge. The maximum electron density at $r = 10$ cm is $10^{20} \pm 2.8 \times 10^{9}$ m^{-3}, $7.2 \times 10^{20} \pm 1.3 \times 10^{20}$m^{-3}, $1.3 \times 10^{21} \pm 3.2 \times 10^{20}$ m^{-3} for the 5, 20-, and 40-J discharge, respectively. The large scatter in the 5-J discharge data is associated with the current measurements being in the low end of sensitivity of the current probes.

The ion speeds can also be evaluated from

$$U_i(t) = S_i(t)\sqrt{kT_e(t)/m_i} \tag{27}$$

assuming an ion with mass of $m_i = 16.66 m_p$. These ion speeds are plotted in Fig. 12 for various distances on the centerline for $E_D = 5$, 20, and 40 J. Figure 12 shows that the ion speed varies during the discharge and exhibit peaks especially prominent at the $r = 10$ cm location. For the 20-J discharge energy the ion speed is approximately 25,800 m/s at $t = 3.12$ μs and decreases to 6800 m/s at $t = 13.04$ μs. For the 40-J discharge energy the ion speed is approximately 24,800 m/s at $t = 3.12$ μs and decreases to 12,200 m/s at $t = 13.04$ μs. These near-exit measurements indicate that the process of ion acceleration in the PPT channel is unsteady with faster ions appearing at the beginning of the discharge. The speed of the ions increases with downstream distance for the 20-J and 40-J discharges because of the expansion of the ions. The magnitudes of the ion speeds depicted in Fig. 12 are consistent with previous measurements reviewed in the introduction, but the present study offers an expanded insight on the ion-speed properties in the PPT plume.

Finally, to validate the quadruple-probe method Fig. 13 shows a comparison between the electron temperature and density for the 40-J discharge with values derived from the current-mode triple-Langmuir-probe measurements of Byrne.[39] This comparison demonstrates the good quantitative and qualitative agreement between the plasma parameters derived independently by these two techniques.

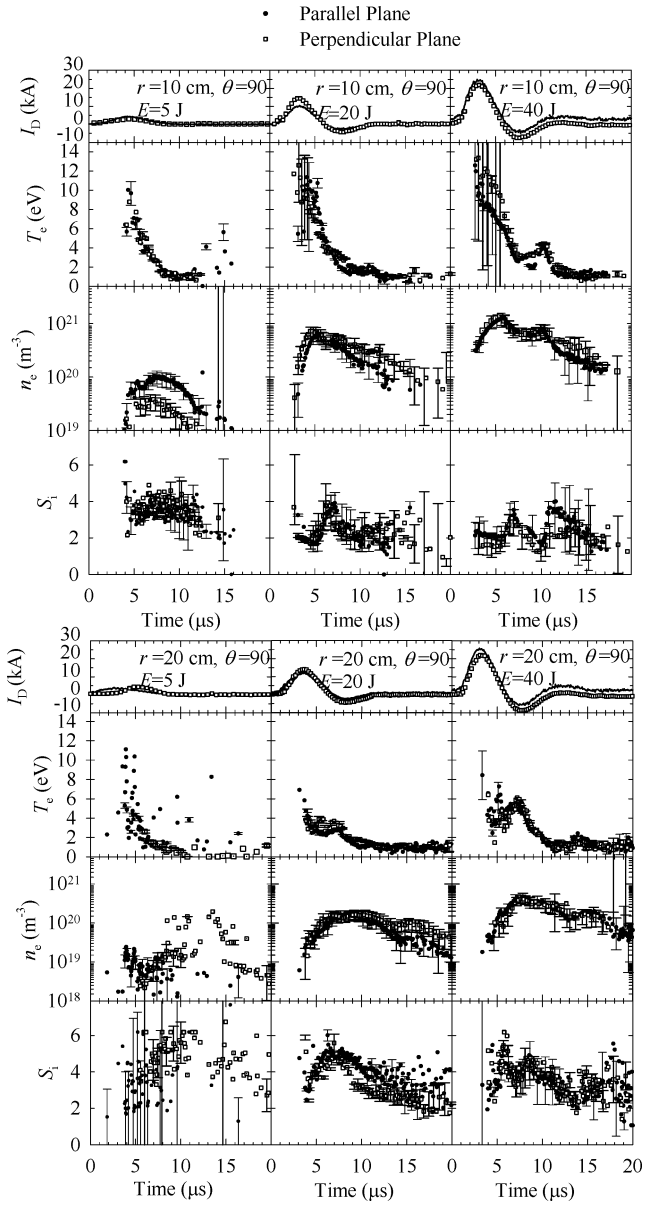

Fig. 11 Electron density, electron temperature, and ion-speed ratio $n_e(t)$, $T_e(t)$, $S_i(t)$ at $r = 10$, $r = 20$ cm, and $\theta = 90$ deg in the plume of a laboratory PPT operating at discharge energies of 5, 20, and 40 J.

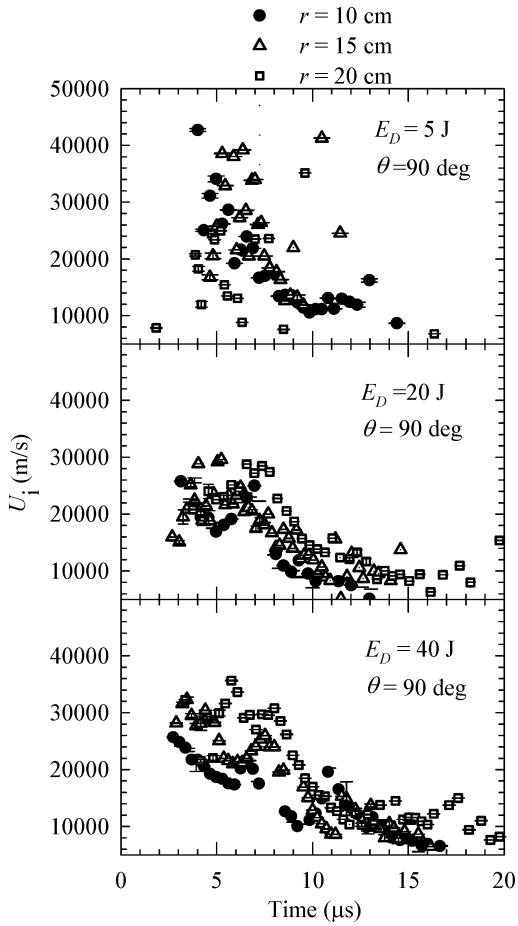

Fig. 12 Ion speeds at centerline in the plume of a 5, 20, and 40-J laboratory PPT.

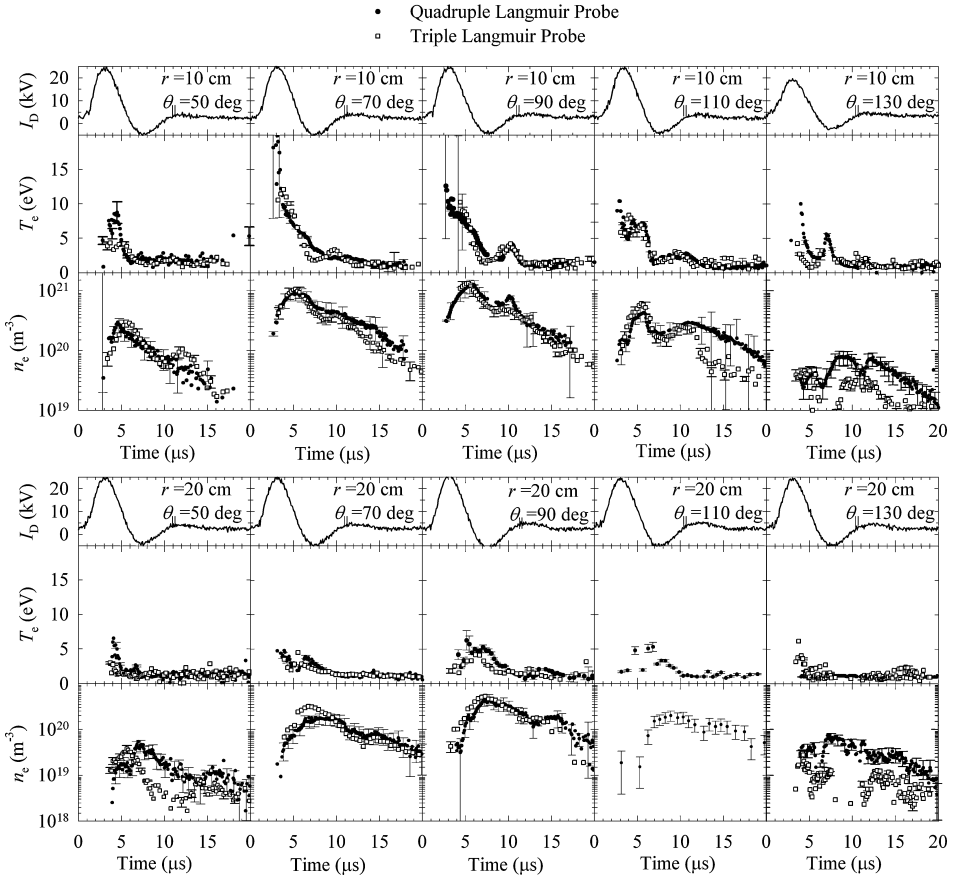

Fig. 13 Electron temperature and density from quadruple-and triple-Langmuir-probe measurements in the plume of a 40-J laboratory PPT.

Conclusions

In the present work a current-mode quadruple-probe method was developed and applied to a pulsed plasma thruster plume to obtain the electron temperature, electron density, and ion-speed ratio. The current-mode operation of the Langmuir-probe operation does not require voltage measurements in the unsteady and fluctuating PPT plume. The implementation incorporates for the parallel to the flow electrodes Laframboise's[26] current-collection theory for $r_p/\lambda_D \leq 100$ and the thin-sheath current collection theory[18] for $r_p/\lambda_D > 100$. The current collection to the perpendicular probe is based on Kanal.[19] In addition, an uncertainty analysis was developed for the nonlinear system of equations that describe the quadruple-current-collection theory.

Data were collected at 10, 15, and 20 cm from the Teflon bar on planes perpendicular and parallel to the electrodes for angles of up to 40 deg from the centerline. The fidelity of the probe technique allowed measurements to be taken during the entire discharge that lasts typically about 15 μs. The measurements show hot electrons of up to 18 eV associated with the peak current during the capacitor discharge. For the most part of the pulse, the electron temperatures remain below 5 eV. The measurements show that electron temperatures decrease with increasing distance from the Teflon propellant while ion-speed ratios increase with increasing downstream distance. The ion speeds estimated for various distances at the centerline decrease during the pulse. This character is indicative of the unsteady acceleration mechanism inside the PPT channel. The data show the temporal and spatial variation of the electron density, electron temperature, and ion-speed ratio during the discharge and provide a complete view of fundamental plasma parameters in the PPT plume.

Acknowledgments

This work was funded in part by NASA Grant NAG3-1873. The authors recognize the contributions of Jim Nichols and Mike Swiatek of NASA Glenn Research Center for their support and assistance during experimentation.

References

[1]Ebert, W. L., Kowal, S. J., and Sloan, R. F., "Operational Nova Spacecraft Teflon PPT System," AIAA Paper 89-2497, July 1989.

[2]Guman, W. J., and Nathanson, D. M., "Pulsed Plasma Microthruster Propulsion System for Synchronous Orbit Satellite," *Journal of Spacecraft and Rockets*, Vol. 7, No. 4, 1970, p. 409.

[3]Arrington, L., Benson, S., Hoskins, W., and Meckel, N., "Development of a PPT for the EO-1 Spacecraft," AIAA Paper 99-2276, June 1999.

[4]Vondra, R. J., Thomassen, K., and Solbes, A., "Analysis of Solid Teflon Pulsed Plasma Thruster," *Journal of Spacecraft and Rockets*, Vol. 7, No. 12, 1970, pp. 1402–1406.

[5]Thomassen, K. I., and Vondra, R. J., "Exhaust Velocity Studies of a Solid Teflon Pulsed Plasma Thruster," *Journal of Spacecraft and Rockets*, Vol. 9, No. 1, 1972, pp. 61–64.

[6]Thomassen, K. I., and Tong, G., "Interferometric Density Measurements in the Arc of a Pulsed Plasma Thruster," *Journal of Spacecraft and Rockets*, Vol. 10, No. 3, 1973, pp. 163–164.

[7]Guman, W. J., and Begun, M., "Exhaust Plume Studies of a Pulsed Plasma Thruster," AIAA Paper 97-704, April 1977.

[8]Rudolph, L. K., Harstad, K. G., Pless, L. C., and Jones, R. M., "Plume Characterization of a One-Millipound Solid Teflon Pulsed Plasma Thruster," U.S. Air Force Rocket Propulsion Lab., TR-79-60, NASA CR-162786, Sept. 1979.

[9]Hirata, M., and Murakami, H., "Exhaust Gas Analysis of a Pulsed Plasma Engine," AIAA Paper 84-52, May 1984.

[10]Myers, R. M., Arrington, L. A., Pencil, E. J., Carter, J., Heminger, J., and Gatsonis, N. A., "Pulsed Plasma Thruster Contamination," AIAA Paper 96-2729, July 1996.

[11]Gatsonis, N. A., Eckman, R., Yin, X., Pencil, E. J., and Myers, R. M., "Experimental Investigations and Numerical Modeling of Pulsed Plasma Thruster Plumes," *Journal of Spacecraft and Rockets*, Vol. 38, No. 3, 2001, pp. 454–464.

[12]Arrington, L. A., and Haag, T. W., "Multi-Axis Thrust Measurement of the EO-1 PPT," AIAA Paper 99-2290, June 1999.

[13]Arrington, L. A., Marrese, C. M., and Blandino, J. J., "Pulsed Plasma Thruster Plume Study: Symmetry and Impact on Spacecraft Surfaces," AIAA Paper 2000-3262, July 2000.

[14]Spanjers, G. G., Lotspeich, J. S., McFall, K. A., and Spores, R. A., "Propellant Losses Because of Particulate Emission in a Pulsed Plasma Thruster," *Journal of Propulsion and Power*, Vol. 14, No. 4, 1998, pp. 554–559.

[15]Eckman, R. F., Byrne, L., Gatsonis, N. A., and Pencil, E. J., "Triple Langmuir Probe Measurements in the Plume of a Pulsed Plasma Thruster," *Journal of Propulsion and Power*, Vol. 17, No. 4, 1998, pp. 554–559.

[16]Dawbarn, R., McGuire, R. L., Steely, S. L., and Pipes, J. G., "Operating Characteristics of an Ablative Pulsed Plasma Thruster," Arnold Engineering Development Center, TR-82-9,1982.

[17]Myers, R. M., Oleson, S., McGuire, M., Meckel, N., and Cassady, R. J., "Pulsed Plasma Thruster Technology for Small Satellite Missions," NASA CR 198427, Nov. 1995.

[18]Chen, S., and Sekiguchi, T., "Instantaneous Direct-Display System of Plasma Parameters by Means of Triple Probe," *Journal of Applied Physics*, Vol. 26, No. 8, 1965, pp. 2363–2375.

[19]Kanal, M., "Theory of Current Collection of Moving Cylindrical Probes," *Journal of Applied Physics*, Vol. 35, No. 6, 1964, pp. 1697–1703.

[20]Johnson, B., and Murphree, D., "Plasma Velocity Determination by Electrostatic Probes," *AIAA Journal*, Vol. 7, No. 10, 1969, pp. 2028–2030.

[21]Poissant, G., and Dudeck, M., "Velocity Profiles in a Rarafied Plasma Stream by Crossed Electrostatic Probes," *Journal of Applied Physics*, Vol. 58, No. 5, 1985, pp. 1772–1779.

[22]Burton, R. L., DelMedico, S. G., and Andrews, J. C., "Application of a Quadruple Probe Technique to MPD Thruster Plume Measurements," *Journal of Propulsion and Power*, Vol. 9, No. 5, 1993, pp. 771–777.

[23]Burton, R. L., and Bufton, S. A., "Exit Plane Electrostatic Probe Measurements of a Low Power Arcjet," *Journal of Propulsion and Power*, Vol. 12, No. 6, 1996, pp. 1099–1106.

[24]Burton, S. A., Bushman, S. S., and Burton, S. A., "Heating and Plasma Properties in a Coaxial Gasdynamic Pulsed Plasma Thruster," *Journal of Propulsion and Power*, Vol. 17, No. 5, 2001, pp. 959–966.

[25]Peterson, E. W., and Talbot, L., "Collisionless Electrostatic Single-Probe and Double-Probe Measurements," *AIAA Journal*, Vol. 8, No. 12, 1970, pp. 2215–2219.

[26]Laframboise, J., "Theory of Cylindrical and Spherical Langmuir Probes in a Collisionless Plasma at Rest," UTIAS Rept. 100, Univ. of Toronto, Inst. of Aerospace Studies, National Technical Information Service Document AD 634596, Springfield, Virginia, June 1966.

[27]Lam, S. H., "Unified Theory for the Langmuir Probe in a Collisionless Plasma," *The Physics of Fluids*, Vol. 8, No. 1, 1965, pp. 73–87.

[28]Byrne, L., Gatsonis, N. A., and Pencil, E., "Triple Langmuir Probe Measurements in the Plume and Backflow Region of a Pulsed Plasma Thruster," AIAA Paper 2001-3640, July 2001.

[29]Lieberman, M. A., and Lichtenberg, A. L., *Principles of Plasma Discharges and Materials Processing*, Wiley, New York, 1994, p. 165.

[30]Chung, P. M., Talbot, L., and Touryan, K. J., "Electric Probes in Stationary and Flowing Plasmas: Part 1. Collisionless and Transitional Probes, and Part 2. Continuum Probes," *AIAA Journal*, Vol. 12, No. 2, 1974, pp. 133–154.

[31]Bruce, C., and Talbot, L., "Cylindrical Electrostatic Probes at Angles of Incidence," *AIAA Journal*, Vol. 13, No. 9, 1975, pp. 1236–1238.

[32]Kirchoff, R. H., Peterson, E. W., and Talbot, L., "An Experimental Study of the Cylindrical Langmuir Probe Response in the Transition Regime," *AIAA Journal*, Vol. 9, No. 9, 1971, pp. 1686–1694.

[33]Coleman, H. W., and Steele, W. G., *Experimentation and Uncertainty Analysis for Engineers*, Wiley, New York, 1999.

[34]*SigmaPlot Users Manual*, SPPS, Inc., Chicago, IL, 1997.

[35]Mitchner, M., and Kruger, C. H., Jr., *Partially Ionized Gases*, Wiley, New York 1973, pp. 385–391.

[36]Mikellides, Y., "Theoretical Modeling and Optimization of Ablation-fed Pulsed Plasma Thrusters," Ph.D. Dissertation, Ohio State Univ., Columbus, OH, 1999.

[37]Sutton, G., and Sherman, A., *Engineering Magnetohydrodynamics*, McGraw–Hill, New York, 1965, pp. 145–149.

[38]Zwahlen, Jurg, "Investigation or a Pulsed Plasma Thruster Plume Using a Quadruple Langmuir Probe Technique," Master's Thesis, Worcester Polytechnic Inst., MA, Nov. 2002.

[39]Byrne, Larry, "Langmuir Probe Measurements in the Plume of a Pulsed Plasma Thruster," M.S. Thesis, Worcester Polytechnic Inst., Nov. 2002.